Hepatic adropin is regulated by estrogen and contributes to adverse metabolic phenotypes in ovariectomized mice

Joshua Stokar [1,4], Irina Gurt [1,4], Einav Cohen-Kfir [1,6], Oran Yakubovsky [1,5], Noa Hallak [1,7], Hadar Benyamini [2], Natan Lishinsky [1], Neta Offir [1], Joseph Tam [3], Rivka Dresner-Pollak [1,*]

ABSTRACT

Objective: Menopause is associated with visceral adiposity, hepatic steatosis and increased risk for cardiovascular disease. As estrogen replacement therapy is not suitable for all postmenopausal women, a need for alternative therapeutics and biomarkers has emerged.

Methods: 9-week-old C57BL/6 J female mice were subjected to ovariectomy (OVX) or SHAM surgery (n = 10 per group), fed a standard diet and sacrificed 6- & 12 weeks post-surgery.

Results: Increased weight gain, hepatic triglyceride content and changes in hepatic gene expression of *Cyp17a1, Rgs16, Fitm1* as well as *Il18, Rares2, Retn, Rbp4* in mesenteric visceral adipose tissue (VAT) were observed in OVX vs. SHAM. Liver RNA-sequencing 6-weeks post-surgery revealed changes in genes and microRNAs involved in fat metabolism in OVX vs. SHAM mice. Energy Homeostasis Associated gene (*Enho*) coding for the hepatokine adropin was significantly reduced in OVX mice livers and strongly inversely correlated with weight gain (r = −0.7 p < 0.001) and liver triglyceride content (r = −0.4, p = 0.04), with a similar trend for serum adropin. *In vitro*, *Enho* expression was tripled by 17β-estradiol in BNL 1 ME liver cells with increased adropin in supernatant. Analysis of open-access datasets revealed increased hepatic *Enho* expression in estrogen treated OVX mice and estrogen dependent ERα binding to *Enho*. Treatment of 5-month-old OVX mice with Adropin (i.p. 450 nmol/kg/ twice daily, n = 4,5 per group) for 6-weeks reversed adverse adipokine gene expression signature in VAT, with a trended increase in lean body mass and decreased liver TG content with upregulation of *Rgs16*.

Conclusions: OVX is sufficient to induce deranged metabolism in adult female mice. Hepatic adropin is regulated by estrogen, negatively correlated with adverse OVX-induced metabolic phenotypes, which were partially reversed with adropin treatment. Adropin should be further explored as a potential therapeutic target and biomarker for menopause-related metabolic derangement.

1. INTRODUCTION

Menopause defined as the permanent cessation of menstruation resulting from the loss of ovarian follicular activity [1], is associated with a deranged metabolic phenotype including weight gain, visceral adiposity, liver steatosis and insulin resistance resulting in a significantly increased risk of developing type 2 diabetes (T2D) and cardiovascular disease (CVD) in post-versus pre-menopausal women [2]. Weight gain results primarily from decreased energy expenditure rather than increased food intake [3,4]. There is a shift in adipose tissue distribution from a lower body predominant subcutaneous fat depot towards a more visceral abdominal distribution pattern [5,6]. Increased visceral adiposity is associated with adipocyte hypertrophy and secretion of adipokines and pro-inflammatory cytokines implicated in insulin resistance and CVD pathogenesis [7—9]. Fat oxidative capacity in the liver and skeletal muscle is reduced resulting in excessive lipid accumulation and increased insulin resistance [10]. As a major metabolic organ as well as a target of the metabolic syndrome, the liver appears to play an important role in mediation of metabolic changes associated with menopause. Known direct liver involvement

[1]Department of Endocrinology and Metabolism, Division of Medicine, Hadassah Medical Organization, Faculty of Medicine, Hebrew University of Jerusalem, Israel [2]Info-CORE, Bioinformatics Unit of the I-CORE at the Hebrew University and Hadassah Medical Center, Jerusalem, Israel [3]Obesity and Metabolism Laboratory, The Institute for Drug Research, School of Pharmacy, Faculty of Medicine, Hebrew University of Jerusalem, Israel

[4] Joshua Stokar and Irina Gurt contributed equally to this work.

[5] OY present affiliation: Department of Molecular Cell Biology, Weizmann Institute of Science, Rehovot, Israel.

[6] ECK present affiliation: Institute of Medical Research Israel—Canada, Hebrew University-Hadassah Medical School, Jerusalem, Israel.

[7] NH present affiliation: Sourasky Medical Center, Tel Aviv, Israel.

*Corresponding author. Department of Endocrinology and Metabolism, Hadassah-Hebrew University Medical Center, P.O.B. 12000, Jerusalem, 91120, Israel. Fax: +97226437940. E-mail: rivkap@mail.huji.ac.il (R. Dresner-Pollak).

Abbreviation: OVX, ovariectomy

includes hepatic steatosis [11], inflammation [12], decreased fatty acid oxidation [13], and increased hepatic glucose production [14].

Studies in women with natural or iatrogenic premature cessation of ovarian function have shown that estrogen depletion and the disruption of estrogen signaling are key factors in menopause-related metabolic dysfunction [15]. However, the benefits and harms of estrogen replacement therapy (ERT) are still a matter of controversy and ERT is not suitable for all women [16].

Historically, recommendations for prevention and treatment of cardiometabolic derangement in postmenopausal women were derived from studies conducted primarily in men. Moreover, pre-clinical biomedical research in animals did not have equal representation of females, reportedly due to the higher susceptibility of males to high fat diet (HFD)-induced metabolic dysfunction [17]. However, a growing body of evidence shows clear sexual dimorphism in metabolic homeostasis with distinct sex- and gender-specific cardio-metabolic phenotypes [6,18,19]. In addition to sex-hormones, there are sex differences in gene expression and networks that impact sex-specific metabolic phenotypes [20,21]. With a mean age at menopause of 50 and life expectancy over 90 years, women in developed countries are expected to spend nearly half their lives in the post-menopausal state [22]. There is an urgent need to discover new biomarkers and therapeutic targets to alleviate metabolic derangement in this rapidly growing population.

Using RNA-sequencing from liver tissue of a mouse model for human menopause (ovariectomy, OVX), we revealed new players in OVX-induced metabolic abnormalities. To separate the effects of sex hormone deficiency from those of aging and obesity, studies were conducted in young adult female mice fed a standard diet.

2. RESULTS

2.1. OVX induced weight gain, pro-inflammatory and adverse adipokine gene expression in VAT and increased hepatic TG content and related genes

The study design is depicted in Figure 1A. Baseline body weight did not differ between SHAM and OVX mice (Figure 1B), and uterine weight was significantly lower in OVX mice, confirming successful OVX-induced suppression of endogenous estrogen production (Figure 1C). Weight gain in OVX mice was significantly higher than in SHAM mice over the course of 12 weeks post-surgery and approached forty percent from baseline (Figure 1D). A significant increase in gene expression of pro-inflammatory cytokines and adipokines was found in VAT of OVX compared to SHAM mice 6-weeks post-surgery
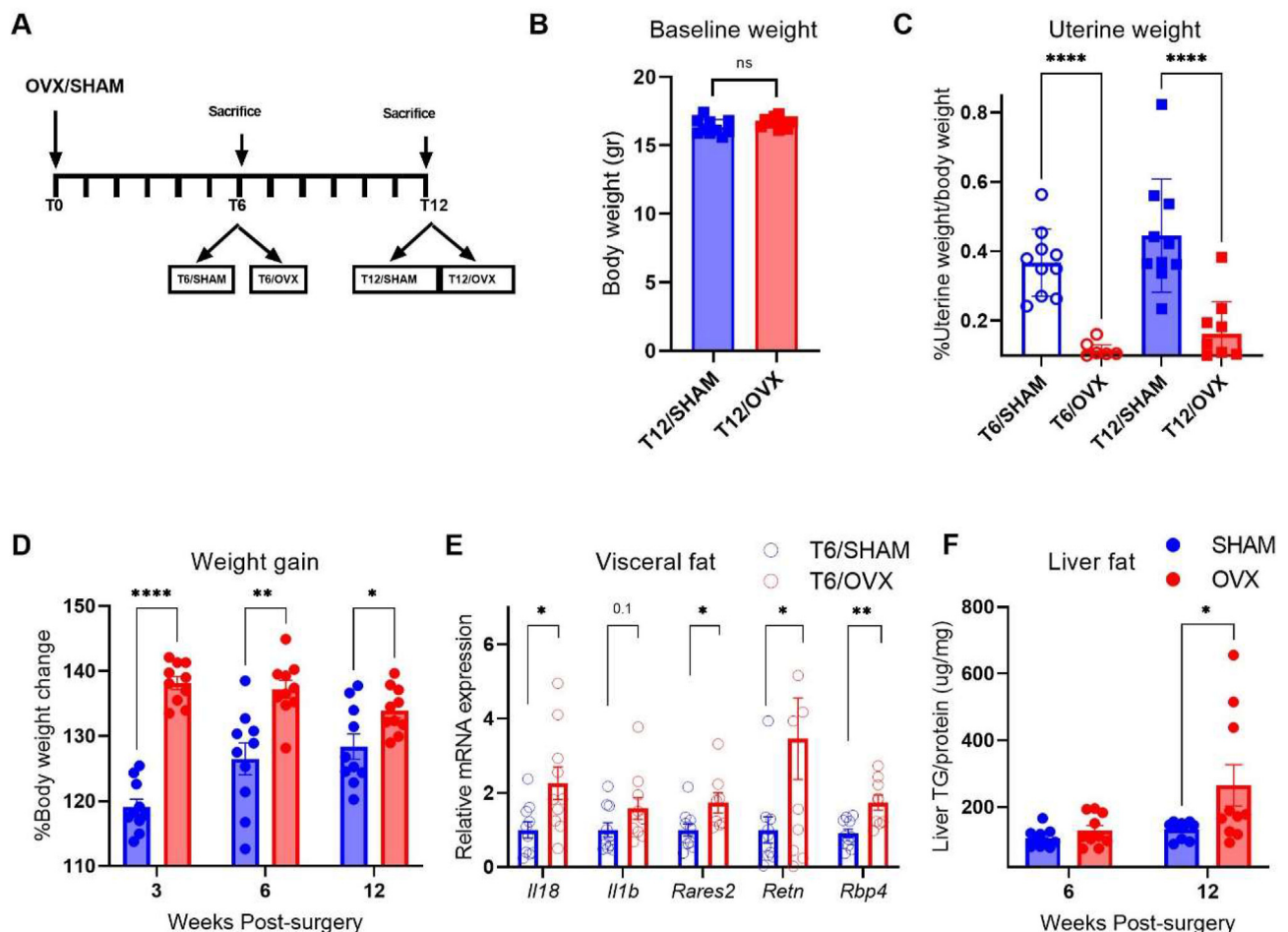

Figure 1: OVX induced weight gain, adverse changes in mesenteric visceral adipose tissue (VAT) and liver. (A) Study design. (B) Body weight at baseline. (C) Uterine weight as percent of body weight. (D) Percent body weight change from baseline. (E) Gene expression of pro-inflammatory cytokines and adipokines in VAT in SHAM and OVX mice at 6 weeks post-surgery. (F) Liver triglyceride (TG) content at 6- and 12-weeks post-surgery. (A—F) n = 10 mice/group. (E) determined by qPCR normalized to geometric mean of *Gapdh*, *actB* and *Polr2a*. Results are Mean ± SEM; Data analyzed by unpaired two-sided *t*-test (B,E) or one-way ANOVA with Sidak's post-hoc correction (C,D,F), *P < 0.05; **P < 0.01; ***P < 0.001 vs. SHAM.

(Figure 1E). Gene expression of Interleukin 18 (*Il18*), Retinoic acid receptor responder protein 2 (*Rarres2*), Resistin (*Retn*) and Retinol Binding Protein 4 (*Rbp4*) were significantly higher in T6/OVX vs. T6/SHAM mice, with a similar trend for Interleukin 1 b (*Il1b*). Hepatic triglyceride (TG) content was increased more than 2-fold in OVX compared to SHAM mice 12 weeks post-surgery (Figure 1F). These findings show that OVX, without additional insult, is sufficient to induce a deranged metabolic phenotype relevant to menopause in young adult female mice and can thus serve as a model to further investigate the molecular mechanisms of OVX-induced metabolic derangement.

2.2. OVX induced transcriptional changes in gene sets for fat metabolism in the liver

OVX induced hepatic transcriptional changes were assessed in T6/OVX vs. T6/SHAM mice. Principal component analysis (PCA) showed samples cluster by gonadal status and not by technical batch (Figure 2A). The spread of differently expressed genes (DEGs) is seen in the volcano plot (Figure 2B), with a total of 103 DEGs, 35 up and 68 downregulated. A Heatmap of the RNA-seq data shows the overall separation between OVX and SHAM mice, indicating an altered hepatic transcriptional response to OVX (Figure 2C). Gene set enrichment analysis (GSEA) showed upregulation of genes involved in fatty acid metabolism as well as genes involved in TNF-α signaling pathway in OVX compared to SHAM mice (Figure 2D, Figure S1). Select differentially expressed genes related to fat and energy metabolism were chosen for RT-PCR validation as well as for comparison at 12 weeks post-surgery (Figure 2E); *Cyp17a1* codes for a key enzyme in steroid hormone biosynthesis, suppressed in obesity and involved in atherosclerosis and dyslipidemia [23]; Cytochrome P450 family 2, subfamily b, polypeptide 10 (*Cyp2b10*) is known to be activated by estrogen and calorie restriction through the Constitutive Active Receptor (CAR) [24,25]; Fat Storage Inducing Transmembrane Protein 1 (*Fitm1*); G0/G1 Switch 2 (*G0s2*) and Regulator of G-protein signaling 16 (*Rgs16*).

2.3. OVX repressed hepatic expression of Enho coding for adropin

We were particularly intrigued by the significant reduction in hepatic expression of the Energy Homeostasis Associated (*Enho*) gene, observed in OVX compared to SHAM mice 6- and 12-weeks post-surgery (Figure 3A). *Enho* relative expression was significantly inversely correlated with hepatic triglyceride content 12-weeks post-surgery (Figure 3B) with a similar trend within the OVX group alone (r = −0.58, P = 0.07). Interestingly, we found a positive correlation between uterine weight, a reflection of the level of estrogen and hepatic *Enho* expression (Figure 3C). Relative weight gain in OVX and SHAM mice at 6 weeks post-surgery also showed a strong inverse correlation with *Enho* liver mRNA expression (Figure 3D), though driven only by the inter-group differences.

Enho codes for the peptide adropin, a highly conserved hepatokine shown to regulate whole body energy homeostasis [26]. Despite the change in mRNA levels, no differences in hepatic adropin protein level in T6/OVX vs. T6/SHAM or T12/OVX vs. T12/SHAM mice could be detected using ELISA (Figure S2). This pattern is consistent with previous reports [27], and may be explained by adropin being a secreted peptide. Indeed, we found a trend for decreased plasma adropin 28 days after OVX which was negatively correlated with weight gain (Figure 3E,F). Reduced liver *Enho* expression and low serum adropin have been previously reported in the context of obesity [26], but have never been investigated in the context of estrogen deficiency, OVX, menopause or disruption of estrogen signaling.

To understand if *Enho* expression is directly regulated by E2 and not merely a byproduct of changes in body weight or liver fat, we conducted *in vitro* studies in BNL 1 ME murine hepatocytes. We found a 3-fold increase in *Enho* expression in response to E2 administration with an increase in adropin levels in the supernatant (Figure 4A,B).

To further validate our findings of direct regulation of hepatic *Enho* expression by E2, we analyzed relevant publicly available datasets from the Gene Expression Omnibus (GEO). In human cells, E2-treated MCF-7 breast cancer cells showed a significant increase in *ENHO* (Figure 4C). In primary human hepatocytes higher *ENHO* expression was found in cells obtained from females compared to males (Figure 4D), compatible with the sexually dimorphic expression pattern observed in mice [28]. Consistent with our own experimental data, we found decreased liver *Enho* expression in OVX vs SHAM mice both on chow or HFD (Figure 4E) and a marked increase in *Enho* expression following E2 treatment in OVX mice on HFD (Figure 4F).

To gain insight into the potential mechanisms of estrogen regulation of *Enho* we analyzed data from liver ERα knockout (KO) and ERα ChIP-Seq experiments. In mouse livers, *Enho* expression was reduced in ERα KO vs. WT mice (Figure 5A) with a significant peek for ERα binding at *Enho* following E2 treatment (Figure 5B). We found a significant ERα binding peak in the promotor region of *ENHO* in pooled human livers (three males and three female, age 44−73 years, Figure 5C). We could not detect an estrogen responsive element (ERE) near the *Enho* promoter. Enrichment analysis on *Enho* co-expressed genes in our RNA-seq data using ChEA [29] reveled enrichment for targets of retinoid X receptor (RXR) (data not shown), known to form a heterodimer with liver X receptor α (LXR). Notably, LXR was previously reported to negatively regulate adropin *in vitro* and *in vivo* [26].

2.4. Adropin treatment partially reversed OVX induced adverse metabolic changes

To test the hypothesis that reduced liver adropin expression plays a causative role in OVX induced metabolic derangement, we performed a small proof of concept intervention study using previously reported therapeutic doses of adropin, administered for 6-weeks following OVX. As expected, adropin treated mice showed a marked increase in adropin serum level (Figure 6A). Surprisingly, neither vehicle nor adropin treated OVX mice gained total body weight relative to baseline (Figure 6B), possibly due to the significant stress of a prolonged twice daily injection regimen. Nonetheless, the adropin treated mice exhibited a trend towards increased lean mass (Figure 6C) and reduced liver fat (Figure 6D−F) with increased expression of *Rgs16* and reduced expression of the fat transporter cluster of differentiation 36 (*Cd36*) (Figure 6G). Importantly, the adverse adipokine pattern in VAT seen with OVX vs SHAM was partially reversed with a significant reduction in gene expression of *Il1b* and *Retn* and trend for *Il18*, *Rars2*, *Rbp4* in adropin vs. vehicle treated OVX mice (Figure 6H). Stearoyl-CoA desaturase-1 (*Scd1*), a key fat storage gene was downregulated in both visceral and subcutaneous adipose tissues in adropin treated mice (Figure 6G,H). *Scd1* was previously shown to be downregulated by adropin in the liver [26]. We found no significant change in blood glucose levels including following a glucose tolerance test (GTT) in adropin vs vehicle treated mice (Figure S3).

2.5. OVX-induced changes in miRNAs involved in fatty acid metabolism

As miRNAs play a role in post-transcriptional regulation of mRNA, we performed miRNA-seq analysis on the same samples used for the RNA-seq. The relative abundance of specific miRNAs is presented in Figure 3A. We found 48 miRNAs to be differentially expressed in OVX vs. SHAM mice, with 24-up and 24 down-regulated (Figure 7A). Samples clustered by gonadal status (Figure 7B). Pathway enrichment analysis of the predicted targets of the differently expressed
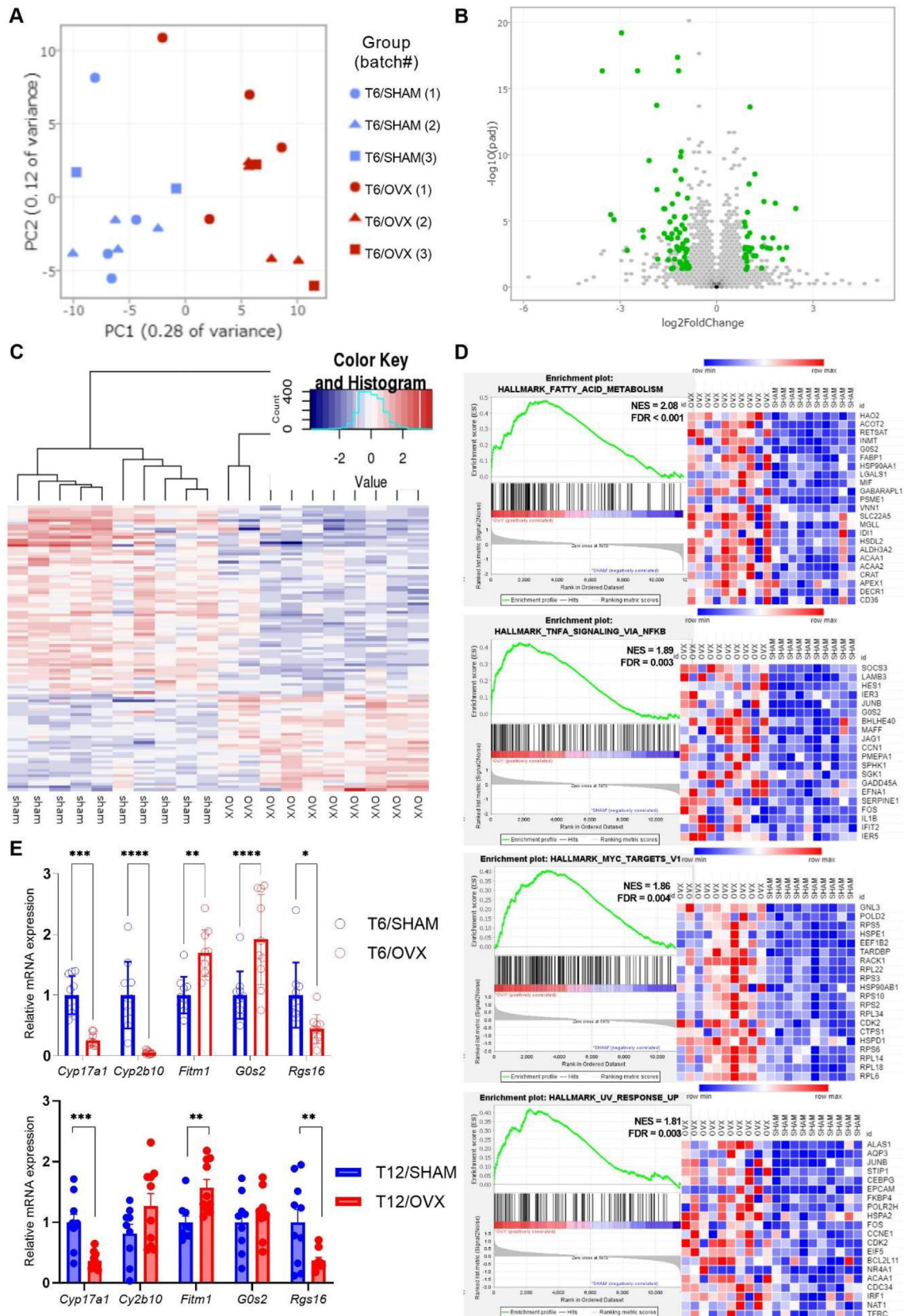
Figure 2: OVX induced liver transcriptional changes 6-weeks post-surgery. (A). Principal component analysis based on top 1000 variably expressed genes. (B) Volcano plot; DEGs (differentially expressed genes) marked in green (fold change ≥ |2|, FDR ≤0.05). (C) Heatmap with hierarchical clustering of DEGs. (D) Top upregulated gene sets by Gene Set Enrichment Analysis by normalized enrichment score (NES) and FDR. (E) Gene expression of key DEGs in liver in SHAM and OVX mice 6-and-12 weeks post-surgery determined by qPCR normalized to geometric mean of *Gapdh*, *actB* and *Polr2a*. Results are Mean ± SEM. Data analyzed by unpaired two-sided *t*-test; *P < 0.05; **P < 0.01; ***P < 0.001; ****P < 0.0001 vs. SHAM. (A—E) n = 10 mice/group.
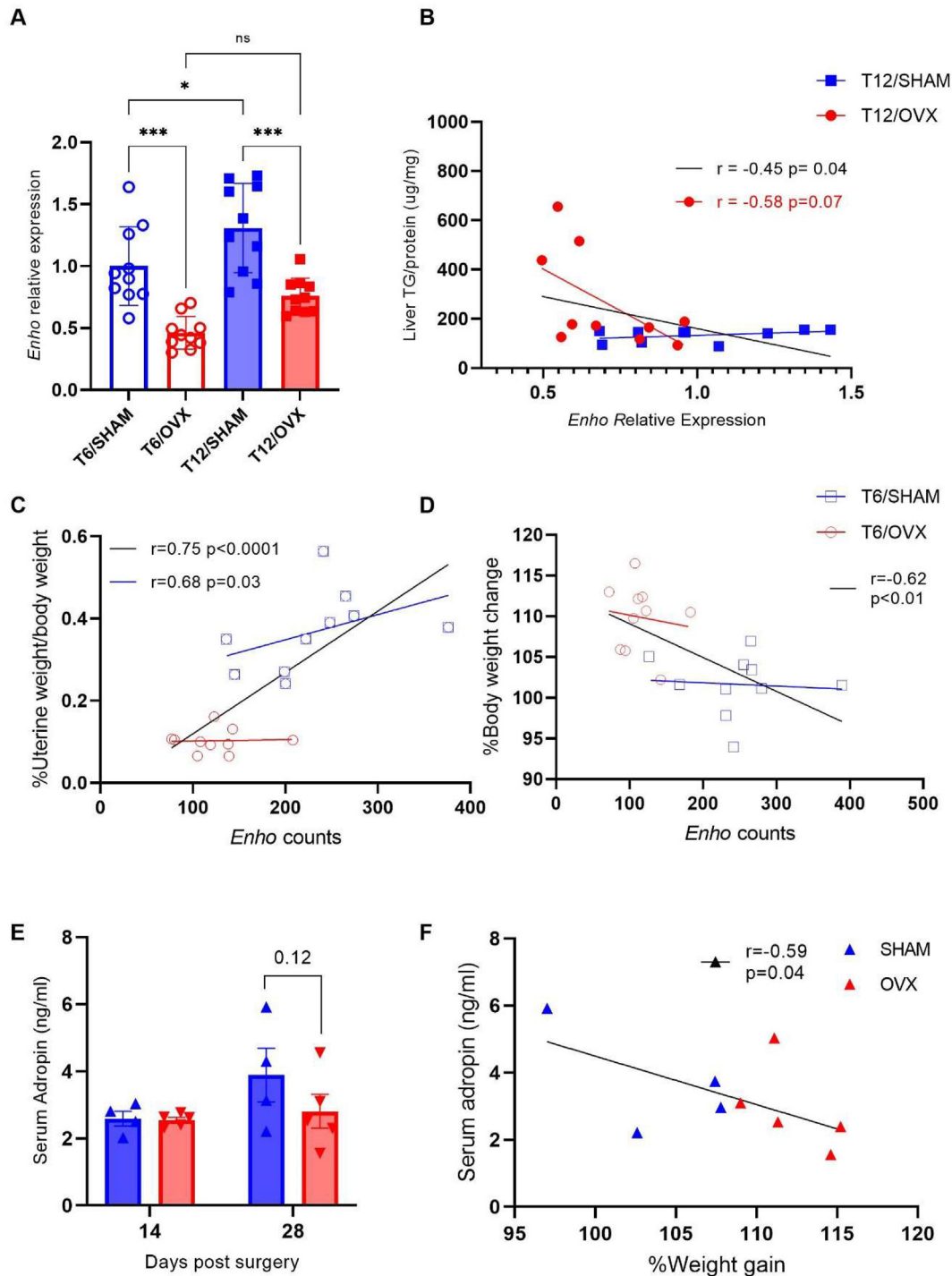
Figure 3: Adropin is negatively correlated with weight gain and liver TG in OVX mice. (A) *Enho* mRNA in liver in OVX and SHAM mice at 6- and 12-weeks post-surgery determined by qPCR normalized to geometric mean of *Gapdh*, *actB* and *Polr2a*. (B) Pearson's correlation and linear regression between liver triglyceride (TG) content and liver *Enho* relative expression at 12 weeks. (C) Pearson's correlation and linear regression between %uterine weight/body weight. (D) Pearson's correlation and linear regression between % weight gain from baseline at 6 weeks and liver *Enho* normalized mRNA count from RNA-seq. (A–D) n = 10 mice/group. (E) Serum adropin in SHAM and OVX mice, 14- and 28-days post-surgery; Results are Mean ± SEM. Data analyzed by unpaired *t*-test. (F) Pearson's correlation and linear regression between serum adropin and %weight gain from baseline 28 days post-surgery. (E–F) n = 4–5 mice/group.

miRNAs revealed enrichment for the KEGG pathways fatty acid biosynthesis and fatty acid metabolism (Figure 7C). We used negative co-expression analysis between previously described miRNA-mRNA pairs to create a miRNA-mRNA network (Figure S4B).

3 of the miRNAs with the most statistically significant differential expression were chosen for validation using RT-PCR (Figure 7D). Liver expression of miRNA-802 and miRNA-455 has been reported to be sexually dimorphic in young adult mice with higher miR-802 and
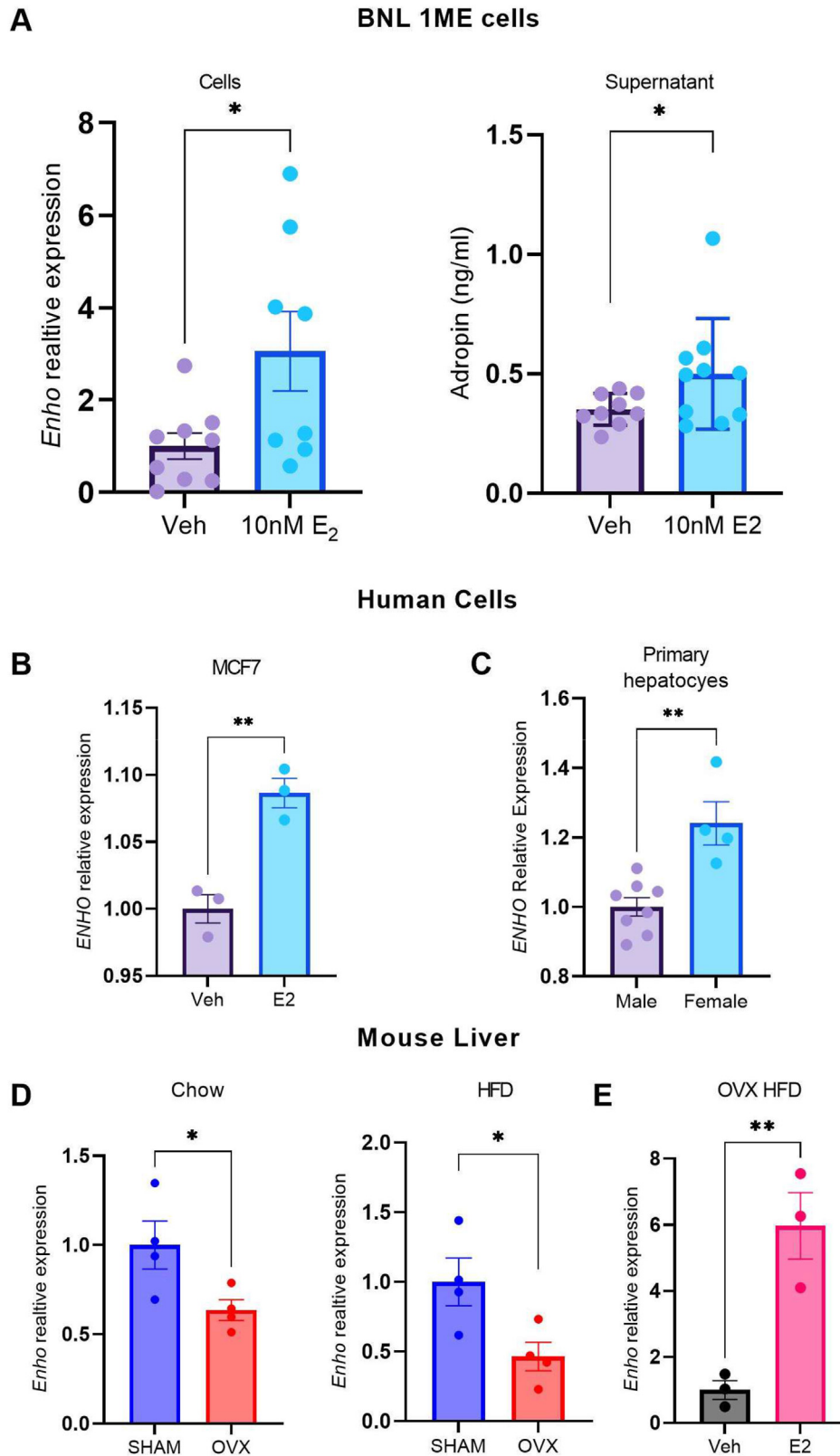
Figure 4: *Enho* expression is regulated by estrogen status. (A) *Enho* mRNA in vehicle- or E2-treated (10 nM) BNL 1 ME cells at 24 h determined by qPCR normalized to geometric mean of *Gapdh*, *actB* and *Polr2a* expression; Adropin level measured in cell supernatant (n = 9 replicates/group) (B) *ENHO* mRNA in MCF7 cell line with or without E2 (GPL4133 at GSE42619, n = 3 replicates/group). (C) *ENHO* mRNA in primary human hepatocytes (GSE17251, data obtained from 2 female and 4 males at 2 time points). (D) *Enho* mRNA in liver from OVX vs SHAM mice (RNA-Seq, GSE112947 n = 4 replicates per group) (E) *Enho* mRNA in liver from OVX mice on HFD treated with VEH (43% DMSO, 15% ethanol, and 42% saline) vs E2, (RNA-seq, GSE92968 n = 3 replicates/group). Results are Mean ± SEM. Data analyzed by unpaired two-sided t-test; *P < 0.05; **P < 0.01; vs. vehicle (A-B, E); vs. male (C); vs. SHAM (D).
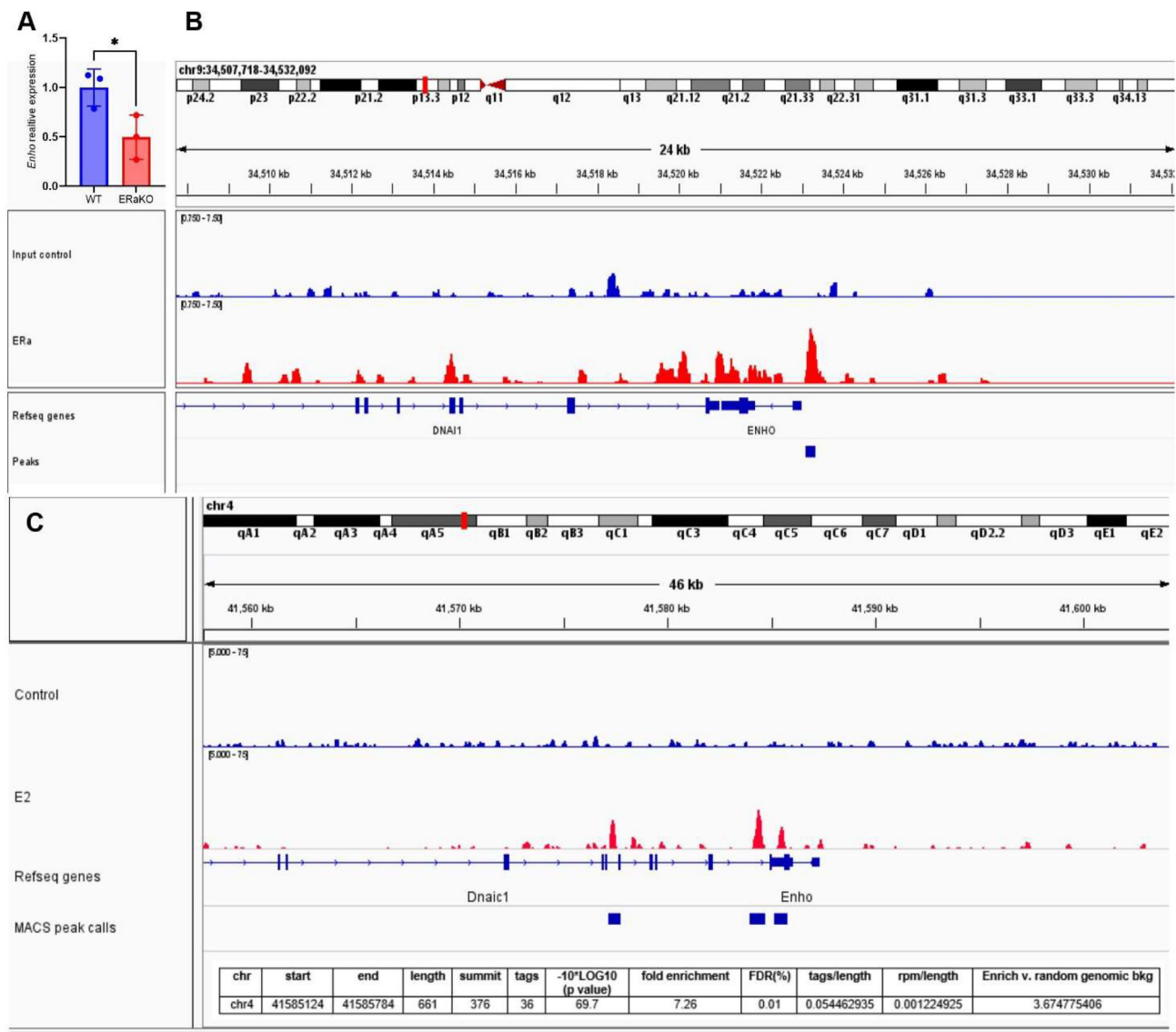
Figure 5: Liver *Enho* expression is regulated via ERα. (A) *Enho* expression in female mouse livers in wild-type (WT) and ERα-knockout (ERαKO) mice (n = 3 per group, GPL1261, GSE95283). Results are Mean ± SEM analyzed by unpaired *t*-test; *P < 0.05 vs. WT mice. (B) ChIP-Seq data for mouse liver ERα binding sites with E2 vs control (GEO GSE52351, n = 5 mice/group). (C) ChIP-Seq data for human liver ERα binding sites (GEO GSE158856, n = 6 samples).

lower miR-455 expression in females vs. males [30]. It seems plausible that the opposite expression pattern we observed in OVX vs. SHAM results from the loss of female sex hormones. miRNA-200a is known to be over-expressed in nonalcoholic fatty liver disease and was previously shown to be up-regulated in OVX mice [31]. Of note, miRNA-29—3p family has been previously reported to regulate hepatic *Enho* expression *in-vivo* in insulin resistant male mice [32], but we found no significant correlation between the two transcripts in OVX and/or SHAM mice (Figure S4A).

3. DISCUSSION

This study demonstrates that OVX without additional insults is sufficient to induce a deranged metabolic phenotype, characteristic of the post-menopausal state including weight gain, increased liver fat and increased gene expression of pro-inflammatory cytokines and unfavorable adipokines in visceral abdominal adipose tissue. While OVX in rodents is often used to study human menopause-related metabolic dysfunction [33], most studies have used older-age, high-fat diet or genetic interventions in addition to OVX to accentuate the deranged phenotype. Our experimental design highlights the net effects of sex-hormone deficiency.

OVX led to increased gene expression of *Il18*, *Rares*, *Retn* and *RBP4* in mesenteric VAT. *Il18* is a pro-inflammatory cytokine from the Il1 family that is increased in visceral adipocytes of obese humans [34] and involved in accelerated atherosclerosis [35]. Increased serum IL18 level was previously reported in post-compared to pre-menopausal women [36]. *Il18* has been shown to be down-regulated by estrogen in multiple tissues [37]. *Rares2* codes for the adipokine chimerin, a regulator of adipocyte development [38] specific to mesenteric fat [39]. Lower serum chimerin level was reported in pre-compared to post-menopausal women [40]. *Retn* codes for the adipokine resistin, a driver of insulin resistance in adipose tissue [41] by inducing pro-inflammatory cytokines production from
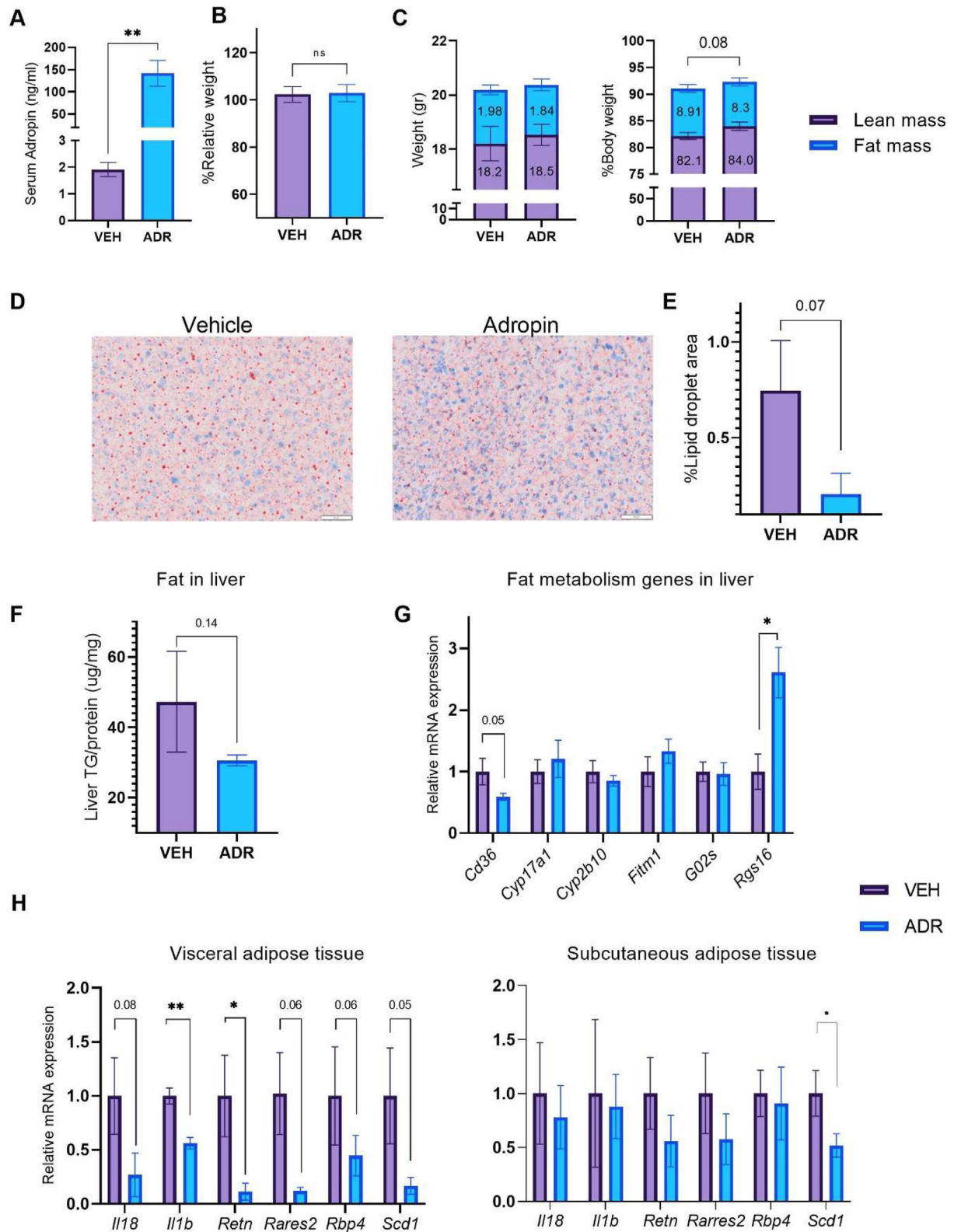
Figure 6: Adropin treatment partially reversed OVX induced metabolic derangement. (A) Serum adropin determined upon sacrifice in adropin and vehicle treated OVX mice 2 h after the last dose. (B) Percent body weight change. (C) Body composition at 4 weeks, p-value for change in lean mass from ANCOVA with total body weight. (D) Representative slides from liver stained with oil-red-o and quantification of lipid droplet area. (F) Liver triglyceride (TG) content. (F) Gene expression of fat metabolism genes in liver. (G) Gene expression of pro-inflammatory cytokines and adipokines in VAT and SCAT; (F,G,H) determined by qPCR normalized to geometric mean of *Gapdh*, *actB* and *Polr2a*. n = 4 mice/group; Results are Mean $\pm$ SEM; Data analyzed by unpaired one-sided *t*-test; *P < 0.05; **P < 0.01 vs. vehicle.
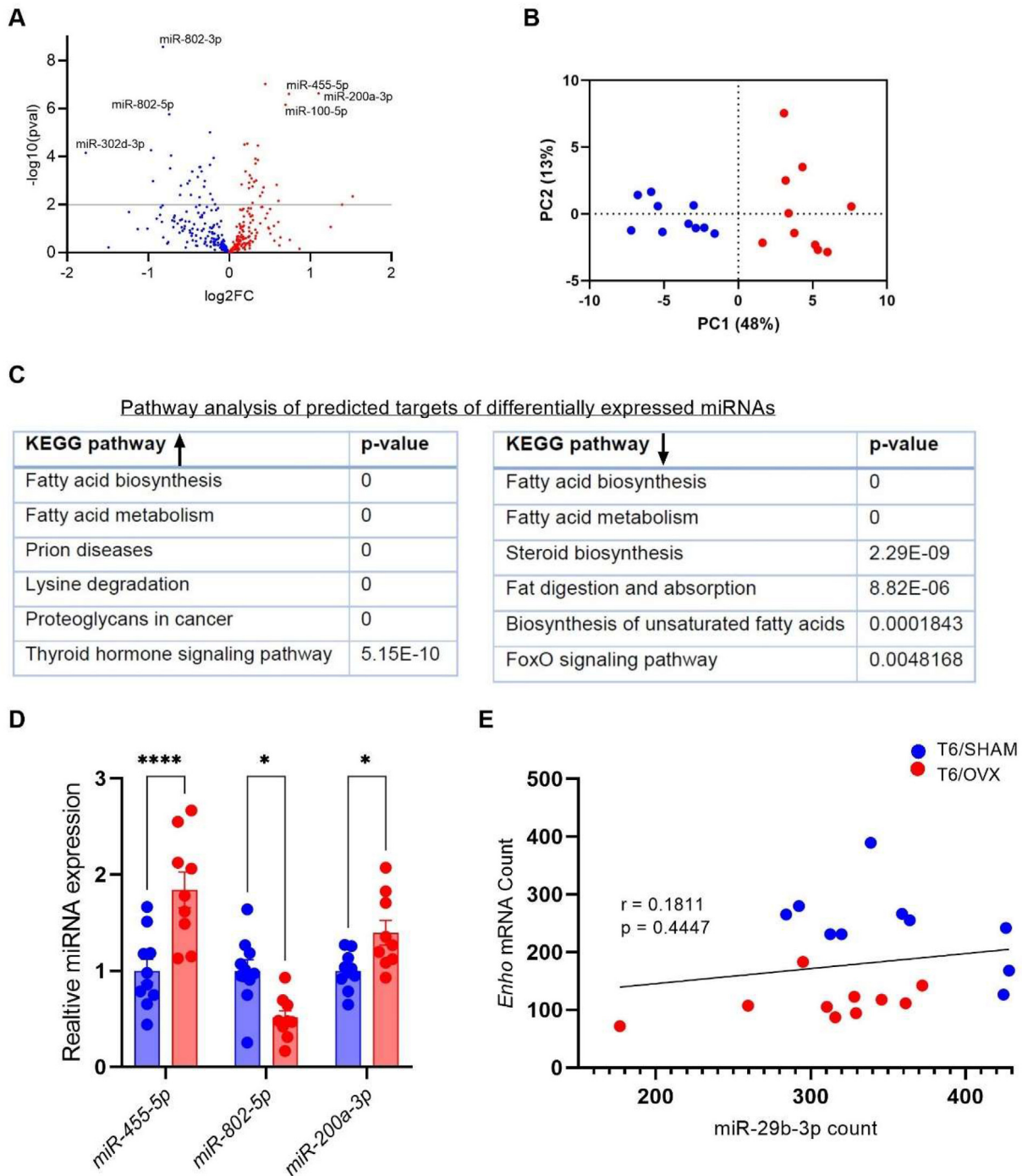
www.molecularmetabolism.com

Figure 7: OVX induced changes in liver miRNA signature 6-weeks post-surgery. (A) Volcano-plot for differently expressed miRNAs (B) PCA analysis of miRNA expression pattern. Top up (C) and downregulated (D) KEGG pathways from targets of differentially expressed miRNA. (D) miRNA expression of select differently expressed miRNAs 6 W post-surgery, determined by qPCR, normalized to the geometric mean expression of $U6$ and $SnoRNA202$. (E) Pearson's correlation and linear regression between liver $Enho$ normalized mRNA count from RNA-seq at 6 W and liver miR-29 b-3p normalized miRNA count from miR-SEQ. Results are Mean $\pm$ SEM (n = 10 mice/group); Data analyzed by unpaired two-sided t-test (C); *$P < 0.05$, ****$P < 0.0001$ vs. SHAM mice.

macrophages residing in adipose tissue [42]. Resistin expression in VAT was shown to be downregulated by estrogen *in-vitro* and *in-vivo* [43], and increased serum resistin was observed in post-menopausal women with the metabolic syndrome compared to those without [44]. *Rbp4* induces inflammation and increased insulin resistance in mice [45]. In humans *RBP4* expression is downregulated by estrogen

in-vivo [46] and exhibits a sexually dimorphic expression pattern in adipose tissue [47].

The liver is a target of the metabolic syndrome but also may play a causative role in menopause-related metabolic derangement. Thus, we focused on transcriptional changes in the liver induced by OVX that occurred prior to the changes observed in liver fat. To our knowledge,

this is the first report of the OVX-induced transcriptional landscape, integrating data from same-sample RNA-seq and miRNA-seq, thus minimizing the effects of sample handling on the data and allowing for establishing co-expression networks. As expected, we discovered significant changes, primarily in gene sets and miRNAs involved in lipid and fatty acid metabolism.

In the liver, OVX induced expression of several genes known to regulate liver fat content: *Fitm1* is a target for Peroxisome proliferator-activated receptor gamma (*Pparγ*), involved in lipid droplet formation and steatohepatitis [48]; *G0s2* is a master regulator of lipid and energy metabolism [49] and *Rgs16* provides a signaling mechanism for glucose production to inhibit G-protein-coupled receptor-stimulated fatty acid oxidation in hepatocytes [50], with a sexually dimorphic expression pattern [28]. Recently, *Rgs16* and *G0s2* have been shown to regulate hepatic substrate oxidation as well as inflammation and fibrosis in livers of obese male mice [51].

Of particular interest is our discovery of reduced liver *Enho* expression in OVX compared to SHAM mice, and its strong inverse correlation with adverse menopause-related clinically important phenotypes, namely weight gain and hepatic steatosis. *Enho* codes for adropin, a conserved 76 amino-acid peptide, highly expressed in the brain. In the liver, adropin is considered a hepatokine, with amino acids 1—33 serving as signal peptide and Adropin[34-76] as the secreted portion [26]. Adropin has both paracrine effects on hepatocytes as well as endocrine effects on muscle and adipocytes. The cell surface receptor for adropin has not yet been characterized, but some studies suggest its effects are mediated via GPR19 [52,53]. Adropin has been implicated in the regulation of glucose and lipid homeostasis mostly in studies conducted in male mice. Adropin-over-expressing male and female mice display milder hepatosteatosis and insulin resistance compared to WT mice when fed HFD [26]. Consistently, male and female adropin knock-out mice exhibit hepatic steatosis, increased serum TG, insulin resistance and increased relative fat mass [54]. Importantly, numerous studies in male mice have investigated the therapeutic potential of Adropin in ameliorating HFD-induced metabolic derangement and have demonstrated beneficial effects in key metabolic organs. Systemic administration of Adropin[34-76] to male WT mice on HFD attenuated liver steatosis and hyperinsulinemia [26], suppressed hepatic gluconeogenesis *in vivo* and *in vitro* [55] and decreased liver fatty acid uptake via downregulation of Cd36 [56], consistent with our results. In another study [57], adropin treatment ameliorated NASH progression by up regulating the expression of Glutamate-Cysteine Ligase Catalytic and Modifier Subunits (Gclc, Gclm) as well as Glutathione Peroxidase 1 (Gpx1) via the factor Nuclear factor erythroid 2-related factor 2 (Nrf2). Other metabolically beneficial effects of adropin have been reported in male mice in skeletal muscle and adipocytes [58,59]. In contrast to the reports regarding the positive effects of adropin on glucose homeostasis [60], in our model, as in post-menopausal women, estrogen depletion does not lead to overt hyperglycemia, which may explain why we found no significant effects of adropin on glucose levels.

In humans, reduced serum adropin has been reported in a wide range of conditions of cardiometabolic dysregulation [61]. Specific polymorphisms in the *ENHO* gene in humans have been described leading to lower serum adropin levels and an increased severity of glucose homeostasis impairment and fat metabolism disorders [62]. In women, lower levels of serum adropin were observed in women with polycystic ovary syndrome, gestational diabetes and endometrial cancer [63—65]. Interestingly, unlike in men, pre-menopausal women exhibited no association between serum adropin and BMI [54] or LDL cholesterol [66]; Though serum adropin was reported to be affected by changes in dietary fat content in young women [67]. To our knowledge, thus far,

only one brief report related serum adropin to menopausal status, where a differential response to meal composition on serum adropin was observed in pre but not post-menopausal women [68].

Known regulators of hepatic adropin are feeding state, nutrients and clock signals [60]. In mice, a short term (2 day) high-fat-diet leads to increased hepatic *Enho* expression, whereas a prolonged HFD (1—3 months) as well as in genetic mouse models of obesity caused by melanocortin receptor or leptin deficiency, liver *Enho* is downregulated [26,66]. In HepG2 cells, adding cholesterol to the culture was shown to downregulate *ENHO*. Treatment with an *LXRα* agonist (GW3965) downregulated *ENHO* in HepG2 cells, while antisense RNA targeting *LXRα* blocked this effect [26,66]. Moreover, lean, chow-fed, male B6 mice treated with an I.V. GW3965 injection exhibited a rapid reduction in hepatic *Enho* expression 4 h after injection [26,66]. Some evidence also points to *Enho* regulation by the circadian clock; Treatment with a Rev-erb agonist was shown to suppress hepatic *Enho in vitro* and *in-vivo* while the RORα/γ inverse agonist (SR1001) suppressed *Enho in-vitro* [26].

To our knowledge this is the first report of *Enho* direct regulation by sex-hormones and its association with OVX-related metabolic derangement. Our findings of *Enho* regulation by estrogen are supported by data we extracted and analyzed from available *in vivo* and *in vitro* studies in mice and humans. Results from these analyses showed increased hepatic *Enho* expression in estrogen-treated vs. untreated OVX HFD mice, upregulation of ENHO in response to 17β-estradiol in a human breast cancer cell line, higher expression in hepatocytes from women vs. men and a genomic ERα binding site by *ENHO* in liver. The mechanisms of hepatic *Enho* regulation by estrogen are elusive and remain to be investigated. LXRα has been shown to directly downregulate hepatic *Enho.* As ERα is known to interact with liver LXRα and inhibit its function [69], a plausible mechanism for *Enho* regulation by estrogen involves ERα repression of LXRα-mediated inhibition of *Enho* transcription. In a recently available dataset, we found reduced hepatic *Enho* expression in OVX vs SHAM both in ERα[f/f] as well as in liver specific ERα knockout (LERKO) mice [70], suggesting additional non-ERα or extra hepatic regulation by estrogen. This is further supported by the reported increase in hepatic *Enho* expression following E2 treatment to LERKO mice [71].

Importantly, using a small proof-of-concept intervention study, we were able to show that adropin reversed some of the metabolic derangement induced by OVX including a trended increase in lean body, a decrease in VAT gene expression of *Il18*, *Il1b*, *Rares*, *Retn* and reduced liver fat with marked upregulation of *Rgs16* gene expression. Larger studies with varying doses and regimens of adropin treatment as well as additional metabolic insults such as HFD seem warranted.

This study has several strengths. By using young adult female OVX mice on a normal diet, we avoided the confounding effects of aging and obesity. Our initial unbiased approach using NGS of the hepatic transcriptome enabled the discovery of a new and potentially druggable player in OVX-induced metabolic abnormalities. Same-sample mRNA and miRNA profiling allowed for direct interaction analysis. We employed a broad-spectrum of experimental methodologies spanning from studies *in-vivo* in the OVX mouse model, *in-vitro* in a murine hepatocyte cell line model, as well as bioinformatic analyses of our own data and in-silico analysis of relevant open-access data. Importantly, our results may have therapeutic implications, as administration of synthetic adropin[36-74] has been shown to improve multiple metabolic parameters, albeit in mostly in male mice. Indeed, in proof-of-concept intervention study we showed that adropin treatment partially reversed deranged phenotypes induced by OVX.

This study is not without limitations. *In-vivo* studies were performed after an overnight fast. As *Enho* liver expression is suppressed by fasting, our results may have underestimated the magnitude of difference in *Enho* and adropin between OVX and SHAM mice. Additionally, the intervention study may have been too small and short to show more significant effects; conversely, prolonged twice daily injections may have put too much stress on the mice.

In conclusion, this study indicates that changes in adropin liver expression may contribute to OVX-induced metabolic derangement and provides a basis for further intervention studies in OVX animals. In a search for new therapies and biomarkers beyond estrogens to improve women's health in the postmenopausal phase, the association between perimenopausal serum adropin level and the changes in metabolic parameters over time in post-menopausal women warrants further evaluation. Finally, although our study was aimed at searching for new targets to alleviate metabolic dysfunction associated with menopause, estrogens and ERα play a role in hepatic steatosis and glucose metabolism also in males and thus our results may be relevant to both sexes [71].

4. METHODS

4.1. Animals & experimental protocol

Forty 8-week-old C57BL/6 J female mice were purchased from Harlan (Rehovot, Israel), housed in constant temperature rooms with 12-hour light/dark cycles and allowed free access to Harlan Teklad chow (2018S) and water. 9-week-old mice were randomly subdivided into 2 groups of bilateral ovariectomy (OVX) and 2 groups of sham surgery (SHAM), (10 animals/group). To allow metabolic changes to occur a group of each OVX and SHAM animals was sacrificed 6- and 12-weeks post-surgery (T6/OVX, T6/SHAM, T12/OVX, T12/SHAM, respectively, Figure 1A). Body weight was determined weekly and uterine weight was determined upon sacrifice to confirm successful OVX. For adropin serum measurement study, five mice underwent OVX and four mice SHAM surgery at 3 months-of-age. Blood from facial vein was drawn at 2- and 4-weeks post-surgery. For adropin treatment study, eight 5-month-old C57BL/6 J female mice underwent OVX and after one week were randomized to receive twice daily intraperitoneal adropin treatment (450 nmol/kg, china peptide company) or vehicle (PBS/0.1% BSA) for 6 weeks. After 4 weeks of treatment, body composition was determined by EchoMRI-100HTM (EchoMedical Systems LLC, Houston, TX, USA). All mice were fasted overnight and killed by CO_2 inhalation. Liver and mesenteric visceral adipose tissue (VAT), the fat pad most analogous to human intra-abdominal VAT [72], were immediately harvested and kept frozen at −80⊠C. The study was approved by The National Council for Animal Experimentation and the Hebrew University ethics committee (approval numbers IL-10-12-113, MD-19-15747-4). All studies were conducted in accordance with ARRIVE guidelines.

4.2. Gene and miRNA expression analysis

RNA was extracted from liver and mesenteric VAT using BIO-TRI RNA (Bio-Lab), reverse transcribed into cDNA (qScript cDNA Synthesis Kit, Quanta Biosciences), and analyzed with SYBR Green-based quantitative RT-PCR. Relative mRNA expression was determined by the comparative CT method. For each sample, the mean cycle threshold (CT) for each gene (run in triplicate) was normalized to the geometric mean of the mean CT of the 3 reference genes (*Gapdh*, *actB* and *Polr2a)* using the formula: $2^{-(\text{gene of interest CT} - \text{reference CT})}$. The resulting

ΔCT for each gene was used to calculate relative gene expression changes between samples. Genes with CT values > 35 were considered not expressed. Supplementary Table 1A provides all the primer sequences used in this study. miRNA-specific cDNA was generated with TaqManTM microRNA Reverse Transcription Kit (4366596, Applied Biosystem). Relative miRNA expression was determined by the comparative CT method and normalized to the geometric mean expression of *U6* (TaqManTM microRNA assay: ID 001973) and *SnoRNA202* (TaqManTM microRNA).

4.3. RNA-sequencing, gene expression profiling and pathway enrichment analysis

RNA was extracted from liver tissue samples of T6/OVX and T6/SHAM mice with QIAGEN miRNeasy Mini Kit (cat. 217004, Qiagen). All RNA samples had an RNA Integrity Number (RIN) of more than 8.1 confirmed by Agilent TapeStation system. RNA libraries were generated with 1ug of RNA as input using the TruSeq RNA Sample Prep kit (Illumina) and poly(A)-enriched according to the TrueSeq protocol. Single-Read 75 reads were sequenced on 4 lanes of an Illumina NextSeq 500. Output was ∼29 million reads per sample. Poly-A/T stretches, and Illumina adapters were trimmed using cutadapt [73]. Resulting reads shorter than 30bp were discarded. Reads were mapped to the *Mus musculus* GRCm38 reference genome using STAR [74] supplied with gene annotations downloaded from Ensembl release 88 with EndToEnd option and outFilterMismatchNoverLmax set to 0.04. Expression levels for each gene were quantified using htseq-count [75]. Analysis of differentially expressed genes between SHAM and OVX mice was performed using DESeq2 [76] with the betaPrior, cooksCutoff and independentFiltering parameters set to False. Principle component analysis (PCA) was performed with DESeq2 package. Heatmaps were created with Morpheus (https://software.broadinstitute.org/morpheus). Gene set enrichment analysis (GSEA) was performed using GSEA and MSigDB [77]. Raw P values were adjusted for multiple testing using the procedure of Benjamini and Hochberg's false discovery rate (FDR q < 0.05)

4.4. Micro-RNA sequencing

micro-RNA (miRNA) sequencing was performed on same liver samples used for RNA-seq. Libraries were prepared using TruSeq Small RNA. SR60 reads were sequenced on 1 lane of an Illumina HiSeq 2500 (v4). Output was ∼9 million reads per sample. Low quality bases were trimmed from the reads using Burrows-Wheeler Alignment [78], adapters were trimmed using cutadapt [73]. Reads were mapped to the mouse genome using Bowtie [79]. Resulting reads shorter than 17bp and longer than 25bp, were discarded. Reads were collapsed into tags for quantification. BLAT was run on tags against 3 blast databases (hairpin, mature and nt). Tags that were not mature miRNA were filtered out, and remained reads were merged by miRNA id. Normalization and differential expression analysis were performed by DESeq2 with the betaPrior, cooksCutoff and independentFiltering parameters set to False. Raw *P* values were adjusted for multiple testing using Benjamini and Hochberg method. GO terms and KEGG Pathway enrichment analysis for DE miRNAs were performed using mirPath v.3 [80]. Experimentally validated miRNA targets were downloaded from DIANA TarBase v8 [81] and visual miRNA-mRNA network were created using cytoscape 3.8 [82] based on a negative significant Pearson's correlation (r ≤ -0.5, p ≤ 0.05). Pathway analysis for miRNA targets was performed using DIANA-miRPath v3. 0 [80], using tarbase as interaction database and Fisher's exact test for KEGG pathway enrichment analysis with FDR correction.

4.5. In vitro studies in the BNL 1 ME murine liver epithelial cell line model

Murine BNL 1 ME liver cells [83] (ATCC®TIB-75) were cultured in Dulbecco's modified eagle medium (DMEM/10% FBS) with a medium change every 3 days. All experiments were conducted in hormone-free medium (charcoal stripped fetal bovine serum; Biological industries, 04-201-1 A). Cells were plated at density of 9×10^5 cells/well and treated with 17β-estradiol (E2) (Calbiochem, #3301) at 10 nM for 24 h. Experiments were performed in triplicates and repeated 3 times. Adropin in cell supernatant was measured using ELISA kit (Phoenix Pharmaceuticals, EK-032-35) according to manufacturer's instructions.

4.6. Liver triglyceride content

Liver triglyceride content was determined by a Triglyceride colorimetric assay (No. 10010303, Cayman Chemical). Triglyceride content was normalized to protein content determined by Bio-Rad Protein Assay (Cat. #500-0006, Bio-Rad).

Liver slides (3 per mouse) were stained using oil-red-o (ab150678, abcam) per manufacturer's instructions. The entire slides were photographed and scanned on Olympus VS200 and automatically analyzed using ImageJ (1.8.0_172) as previously described for quantification of lipid droplet area [84].

4.7. Adropin serum measurement

Serum adropin was measured in duplicates using an EIA kit (EK-032-35, Phoenix Pharmaceuticals) as per manufacturer's instructions.

4.8. Analysis of open access datasets

Expression data for OVX vs SHAM mouse liver on chow and HFD were downloaded from GEO GSE112947. Specific experimental methods were previously published [85]. Briefly, sixteen female C57BL/6 J were maintained on a chow (Ralston Purina Company) or HF/HS diet (Research Diets D12266B) at 8 weeks of age until 16 weeks of age. At 6 weeks of age the mice were ovariectomized or sham operated. Frozen liver tissues were RNA-Seq expression profiling using Illumina HiSeq 2000. We used DESeq2 for differential expression analysis.

Expression data for OVX HFD mouse liver with E2 or vehicle treatment were downloaded from GEO GSE92968. The specific experimental methods were previously published [86]. Briefly, female C57BL/6 J mice were ovariectomized at 8 weeks of age, switched to a high-fat diet (Harlan TD.88137) and divided randomly to vehicle or E2 (0.72 mg, 60-day release E2 pellets, Innovative Research of America) for six weeks till sacrifice. Three liver RNA samples from each treatment group were used for RNA-Seq. Gene expression values quantified from BAM files were calculated using StrandNGS and DESeq normalization. Normalized data was directly available to us for download. We assessed the data for quality control using DSEeq package for R. We used unpaired t-test for *Enho* expression analysis in E2-vs. vehicle-treated mice.

Expression data for mouse ERαKO liver were downloaded from GEO GSE95283. The specific experimental methods were previously published [87]. Briefly, WT and global ERαKO female mice (lacking exon 3 of *Esr1)* were placed on regular ad-libitum diet (NIH-31, Harlan Laboratory) and sacrificed at age 20 weeks. Liver tissue was harvested for RNA extraction and hybridization on GPL1261 Affymetrix Mouse Genome 430 2.0 Array. We assessed raw data for quality control and log2 transformed using the R packages GEOquery, limma and umap. Probe ID 1428739_at was used to obtain normalized *Enho* expression. *Enho* expression in WT vs ERαKO samples was compared using an unpaired t-test.

Expression data in MCF7 cell line were downloaded from GEO GSE42619. The specific experimental methods were previously published [88]. Briefly, MCF-7 cells were cultured for 48 h in medium with 10% charcoal-stripped FBS, and then were treated with or without E2 for 24 h before collection (n = 3 replicates/per group). Gene expression analysis was performed using Agilent-014850 Whole Human Genome Microarray. We assessed raw data for quality control and log2 transformed using the R packages GEOquery, limma and umap. Probe IDs 9947 was used to obtain *ENHO* expression. Unpaired t-test was used to compare *ENHO* expression in between each two pairs of groups.

Expression data in primary human hepatocytes were downloaded from GEO GSE17251. The specific experimental methods were previously published [89]. Briefly, primary hepatocytes were isolated from surgical liver biopsies obtained from six individual donors, 2 females and 4 males. Cells were incubated in fresh medium dissolved in DMSO for 6 and 24 h, followed by RNA isolation and gene expression profiling using Affymetrix Human Genome U133 Plus 2.0 Array. We assessed raw data for quality control and log2 transformed using the R packages GEOquery, limma and umap. Probe ID 228403_at was used to obtain normalized *ENHO* expression. *ENHO* expression in male vs female samples at both time points was compared using an unpaired t-test.

Data for mouse liver ERα ChIP-Seq were downloaded from GEO GSE52351. The specific experimental methods were previously published [90]. Briefly, liver fragments were harvested from 8-week-old female C57/BL6 OVX mice and treated ex vivo with 10 nM E2 or ethanol as vehicle for 45 min in DMEM (n = 5 mice/condition). ChIP-Seq performed with anti-ERa HC-20 antibody (Santa Cruz Biotechnology) and 10 μL of anti-ERa Ab-10 (NeoMarkers). ERα binding peaks were called using Model-based Analysis of ChIP-Seq (MACS) [91]. Data for human liver ERα ChIP-Seq were downloaded from GEO GSE158856. The specific experimental methods were previously published [92]. Briefly, six human liver tissues (three males and three female, age 44−73 yrs) were pooled. ChIP-Seq was performed using a commercial service (Active Motif, Carlsbad, CA, USA) with an anti-ESR1 antibody (sc-543, Santa Cruz Biotech, Dallas, TX, USA). Peaks were called using Homer v4.10 [93]. We used the resulting bedgraph files from both data sets to display significant peaks using the IGV browser for windows (http://software.broadinstitute.org/software/igv/) on top of the mouse (mm9) and human (hg38) genomes, respectively.

4.9. Statistical analysis

Statistical significance was calculated using GraphPad Prism for Windows (GraphPad Software, La Jolla California USA). Outliers were automatically removed using the ROUT method with Q = 1%. Unpaired Student's t-test was used to compare means of 2 groups. To assess differences between multiple means one-way ANOVA followed by Sidak post-hoc correction was performed. Correlation coefficients were calculated with Pearson's correlation analysis. Differences of $P < 0.05$ were considered significant.

AUTHOR CONTRIBUTIONS

JS & IG — planned and conducted experiments, acquired, and analyzed data, wrote and prepared manuscript; ECK, OY, & NH - conducted experiments; HB - analyzed data; NL, NO & JT conducted experiments and analyzed data. RDP — designed research, wrote and prepared manuscript.

CONFLICTS OF INTEREST

The authors have declared no conflicts of interest exist.

APPENDIX A. SUPPLEMENTARY DATA

Supplementary data to this article can be found online at https://doi.org/10.1016/j.molmet.2022.101482.

REFERENCES

[1] Organization, W.H., 1981. Research on the menopause: report of a WHO scientific group [meeting held in Geneva from 8 to 12 December 1980]. World Health Organization.

[2] LeBlanc, E.S., Kapphahn, K., Hedlin, H., Desai, M., Parikh, N.I., Liu, S., et al., 2017 Jan. Reproductive history and risk of type 2 diabetes mellitus in postmenopausal women: findings from the Women's Health Initiative. Menopause 24(1):64—72.

[3] Van Pelt, R.E., Gavin, K.M., Kohrt, W.M., 2015 Sep. Regulation of body composition and bioenergetics by estrogens. Endocrinology and Metabolism Clinics of North America 44(3):663—676.

[4] Marlatt, K.L., Pitynski-Miller, D.R., Gavin, K.M., Moreau, K.L., Melanson, E.L., Santoro, N., et al., 2022. Body composition and cardiometabolic health across the menopause transition. Obesity 30(1):14—27.

[5] Lovejoy, J.C., Champagne, C.M., de Jonge, L., Xie, H., Smith, S.R., 2008 Jun. Increased visceral fat and decreased energy expenditure during the menopausal transition. International Journal of Obesity 32(6):949—958.

[6] Goossens, G.H., Jocken, J.W.E., Blaak, E.E., 2020 Nov. Sexual dimorphism in cardiometabolic health: the role of adipose tissue, muscle and liver. Nature Reviews Endocrinology 10.

[7] Lee, C.G., Carr, M.C., Murdoch, S.J., Mitchell, E., Woods, N.F., Wener, M.H., et al., 2009 Apr. Adipokines, inflammation, and visceral adiposity across the menopausal transition: a prospective study. Journal of Clinical Endocrinology & Metabolism 94(4):1104—1110.

[8] Pfeilschifter, J., Koditz, R., Pfohl, M., Schatz, H., 2002 Feb. Changes in proinflammatory cytokine activity after menopause. Endocrine Reviews 23(1):90—119.

[9] Hong, S.C., Yoo, S.W., Cho, G.J., Kim, T., Hur, J.Y., Park, Y.K., et al., 2007 Sep-Oct. Correlation between estrogens and serum adipocytokines in premenopausal and postmenopausal women. Menopause 14(5):835—840.

[10] Camporez, J.P., Jornayvaz, F.R., Lee, H.Y., Kanda, S., Guigni, B.A., Kahn, M., et al., 2013 Mar. Cellular mechanism by which estradiol protects female ovariectomized mice from high-fat diet-induced hepatic and muscle insulin resistance. Endocrinology 154(3):1021—1028.

[11] Volzke, H., Schwarz, S., Baumeister, S.E., Wallaschofski, H., Schwahn, C., Grabe, H.J., et al., 2007 Apr. Menopausal status and hepatic steatosis in a general female population. Gut 56(4):594—595.

[12] Rogers, N.H., Perfield 2nd, J.W., Strissel, K.J., Obin, M.S., Greenberg, A.S., 2009 May. Reduced energy expenditure and increased inflammation are early events in the development of ovariectomy-induced obesity. Endocrinology 150(5):2161—2168.

[13] Paquette, A., Chapados, N.A., Bergeron, R., Lavoie, J.M., 2009 Jul. Fatty acid oxidation is decreased in the liver of ovariectomized rats. Hormone and Metabolic Research 41(7):511—515.

[14] Nigro, M., Santos, A.T., Barthem, C.S., Louzada, R.A., Fortunato, R.S., Ketzer, L.A., et al., 2014 Aug. A change in liver metabolism but not in brown adipose tissue thermogenesis is an early event in ovariectomy-induced obesity in rats. Endocrinology 155(8):2881—2891.

[15] Muka, T., Oliver-Williams, C., Kunutsor, S., Laven, J.S., Fauser, B.C., Chowdhury, R., et al., 2016 Oct 1. Association of age at onset of menopause and time since onset of menopause with cardiovascular outcomes, intermediate vascular traits, and all-cause mortality: a systematic review and meta-analysis. JAMA Cardiol 1(7):767—776.

[16] Lobo, R.A., 2017 Apr. Hormone-replacement therapy: current thinking. Nature Reviews Endocrinology 13(4):220—231.

[17] Ingvorsen, C., Karp, N.A., Lelliott, C.J., 2017 Apr 10. The role of sex and body weight on the metabolic effects of high-fat diet in C57BL/6N mice. Nutrition & Diabetes 7(4):e261.

[18] Beale, A.L., Nanayakkara, S., Segan, L., Mariani, J.A., Maeder, M.T., van Empel, V., et al., 2019 Mar. Sex differences in heart failure with preserved ejection fraction pathophysiology: a detailed invasive hemodynamic and echocardiographic analysis. JACC Heart Fail 7(3):239—249.

[19] Lagou, V., Magi, R., Hottenga, J.J., Grallert, H., Perry, J.R.B., Bouatia-Naji, N., et al., 2021 Jan 5. Sex-dimorphic genetic effects and novel loci for fasting glucose and insulin variability. Nature Communications 12(1):24.

[20] Heid, I.M., Jackson, A.U., Randall, J.C., Winkler, T.W., Qi, L., Steinthorsdottir, V., et al., 2010 Nov. Meta-analysis identifies 13 new loci associated with waist-hip ratio and reveals sexual dimorphism in the genetic basis of fat distribution. Nature Genetics 42(11):949—960.

[21] Bartz, D., Chitnis, T., Kaiser, U.B., Rich-Edwards, J.W., Rexrode, K.M., Pennell, P.B., et al., 2020 Apr 1. Clinical advances in sex- and gender-informed medicine to improve the health of all: a review. JAMA Internal Medicine 180(4):574—583.

[22] OECD, 2017. Life expectancy by sex and education level.

[23] Tabur, S., Oztuzcu, S., Oguz, E., Demiryurek, S., Dagli, H., Alasehirli, B., et al., 2016 Nov - Dec. CYP gene expressions in obesity-associated metabolic syndrome. Obesity Research & Clinical Practice 10(6):719—723.

[24] Kawamoto, T., Kakizaki, S., Yoshinari, K., Negishi, M., 2000 Nov. Estrogen activation of the nuclear orphan receptor CAR (constitutive active receptor) in induction of the mouse Cyp2b10 gene. Molecular Endocrinology 14(11):1897—1905.

[25] Ding, X., Lichti, K., Kim, I., Gonzalez, F.J., Staudinger, J.L., 2006 Sep 8. Regulation of constitutive androstane receptor and its target genes by fasting, cAMP, hepatocyte nuclear factor alpha, and the coactivator peroxisome proliferator-activated receptor gamma coactivator-1alpha. Journal of Biological Chemistry 281(36):26540—26551.

[26] Kumar, K.G., Trevaskis, J.L., Lam, D.D., Sutton, G.M., Koza, R.A., Chouljenko, V.N., et al., 2008 Dec. Identification of adropin as a secreted factor linking dietary macronutrient intake with energy homeostasis and lipid metabolism. Cell Metabolism 8(6):468—481.

[27] Drew, J.E., Reichardt, N., Williams, L.M., Mayer, C.D., Walker, A.W., Farquharson, A.J., et al., 2018 Oct 22. Dietary fibers inhibit obesity in mice, but host responses in the cecum and liver appear unrelated to fiber-specific changes in cecal bacterial taxonomic composition. Scientific Reports 8(1):15566.

[28] Weger, B.D., Gobet, C., Yeung, J., Martin, E., Jimenez, S., Betrisey, B., et al., 2019. The mouse microbiome is required for sex-specific diurnal rhythms of gene expression and metabolism. Cell Metabolism 29(2):362—382 e8.

Original Article

[29] Lachmann, A., Xu, H., Krishnan, J., Berger, S.I., Mazloom, A.R., Ma'ayan, A., 2010 Oct 1. ChEA: transcription factor regulation inferred from integrating genome-wide ChIP-X experiments. Bioinformatics 26(19):2438—2444.

[30] Hao, P., Waxman, D.J., 2018 Mar 1. Functional roles of sex-biased, growth hormone-regulated MicroRNAs miR-1948 and miR-802 in young adult mouse liver. Endocrinology 159(3):1377—1392.

[31] Feng, Y.Y., Xu, X.Q., Ji, C.B., Shi, C.M., Guo, X.R., Fu, J.F., 2014. Aberrant hepatic microRNA expression in nonalcoholic fatty liver disease. Cellular Physiology and Biochemistry 34(6):1983—1997.

[32] Hung, Y.H., Kanke, M., Kurtz, C.L., Cubitt, R., Bunaciu, R.P., Miao, J., et al., 2019 Aug 1. Acute suppression of insulin resistance-associated hepatic miR-29 in vivo improves glycemic control in adult mice. Physiological Genomics 51(8):379—389.

[33] Medina-Contreras, J., Villalobos-Molina, R., Zarain-Herzberg, A., Balderas-Villalobos, J., 2020 Aug. Ovariectomized rodents as a menopausal metabolic syndrome model. A minireview. Mol Cell Biochem 27.

[34] Ahmad, R., Thomas, R., Kochumon, S., Sindhu, S., 2017 Sep. Increased adipose tissue expression of IL-18R and its ligand IL-18 associates with inflammation and insulin resistance in obesity. Immun Inflamm Dis 5(3):318—335.

[35] Wang, J., Sun, C., Gerdes, N., Liu, C., Liao, M., Liu, J., et al., 2015 Jul. Interleukin 18 function in atherosclerosis is mediated by the interleukin 18 receptor and the Na-Cl co-transporter. Nature Medicine 21(7):820—826.

[36] Cioffi, M., Esposito, K., Vietri, M.T., Gazzerro, P., D'Auria, A., Ardovino, I., et al., 2002 Mar 25. Cytokine pattern in postmenopause. Maturitas 41(3):187—192.

[37] Mansoori, M.N., Shukla, P., Kakaji, M., Tyagi, A.M., Srivastava, K., Shukla, M., et al., 2016 Sep 21. IL-18BP is decreased in osteoporotic women: prevents Inflammasome mediated IL-18 activation and reduces Th17 differentiation. Scientific Reports 6:33680.

[38] Goralski, K.B., McCarthy, T.C., Hanniman, E.A., Zabel, B.A., Butcher, E.C., Parlee, S.D., et al., 2007 Sep 21. Chemerin, a novel adipokine that regulates adipogenesis and adipocyte metabolism. Journal of Biological Chemistry 282(38):28175—28188.

[39] Ferland, D.J., Garver, H., Contreras, G.A., Fink, G.D., Watts, S.W., 2020. Chemerin contributes to in vivo adipogenesis in a location-specific manner. PLoS One 15(2):e0229251.

[40] Menzel, J., Biemann, R., Aleksandrova, K., Schulze, M.B., Boeing, H., Isermann, B., et al., 2018 May. The cross-sectional association between chemerin and bone health in peri/pre and postmenopausal women: results from the EPIC-Potsdam study. Menopause 25(5):574—578.

[41] Steppan, C.M., Bailey, S.T., Bhat, S., Brown, E.J., Banerjee, R.R., Wright, C.M., et al., 2001 Jan 18. The hormone resistin links obesity to diabetes. Nature 409(6818):307—312.

[42] Norseen, J., Hosooka, T., Hammarstedt, A., Yore, M.M., Kant, S., Aryal, P., et al., 2012 May. Retinol-binding protein 4 inhibits insulin signaling in adipocytes by inducing proinflammatory cytokines in macrophages through a c-Jun N-terminal kinase- and toll-like receptor 4-dependent and retinol-independent mechanism. Molecular and Cellular Biology 32(10):2010—2019.

[43] Huang, S.W., Seow, K.M., Ho, L.T., Chien, Y., Chung, D.Y., Chang, C.L., et al., 2005 Jan 17. Resistin mRNA levels are downregulated by estrogen in vivo and in vitro. FEBS Letters 579(2):449—454.

[44] Palla, G., Ramirez-Moran, C., Montt-Guevara, M.M., Salazar-Pousada, D., Shortrede, J., Simoncini, T., et al., 2020 Jun. Perimenopause, body fat, metabolism and menopausal symptoms in relation to serum markers of adiposity, inflammation and digestive metabolism. Journal of Endocrinological Investigation 43(6):809—820.

[45] Moraes-Vieira, P.M., Yore, M.M., Sontheimer-Phelps, A., Castoldi, A., Norseen, J., Aryal, P., et al., 2020 Dec 8. Retinol binding protein 4 primes the NLRP3 inflammasome by signaling through Toll-like receptors 2 and 4. Proceedings of the National Academy of Sciences of the United States of America 117(49):31309—31318.

[46] Jung, U.S., Jeong, K.J., Kang, J.K., Yi, K., Shin, J.H., Seo, H.S., et al., 2013 Sep. Effects of estrogen receptor alpha and beta on the expression of visfatin and retinol-binding protein 4 in 3T3-L1 adipocytes. International Journal of Molecular Medicine 32(3):723—728.

[47] Kos, K., Wong, S., Tan, B.K., Kerrigan, D., Randeva, H.S., Pinkney, J.H., et al., 2011 Feb. Human RBP4 adipose tissue expression is gender specific and influenced by leptin. Clinical Endocrinology 74(2):197—205.

[48] Hasenfuss, S.C., Bakiri, L., Thomsen, M.K., Williams, E.G., Auwerx, J., Wagner, E.F., 2014 Jan 7. Regulation of steatohepatitis and PPARgamma signaling by distinct AP-1 dimers. Cell Metabolism 19(1):84—95.

[49] Zhang, X., Heckmann, B.L., Campbell, L.E., Liu, J., 2017 Oct. G0S2: a small giant controller of lipolysis and adipose-liver fatty acid flux. Biochimica et Biophysica Acta (BBA) - Molecular and Cell Biology of Lipids 1862(10 Pt B): 1146—1154.

[50] Pashkov, V., Huang, J., Parameswara, V.K., Kedzierski, W., Kurrasch, D.M., Tall, G.G., et al., 2011 Apr 29. Regulator of G protein signaling (RGS16) inhibits hepatic fatty acid oxidation in a carbohydrate response element-binding protein (ChREBP)-dependent manner. Journal of Biological Chemistry 286(17): 15116—15125.

[51] Bai, X., Liao, Y., Sun, F., Xiao, X., Fu, S., 2021. Diurnal regulation of oxidative phosphorylation restricts hepatocyte proliferation and inflammation. Cell Reports 36(10).

[52] Stein, L.M., Yosten, G.L., Samson, W.K., 2016 Mar 15. Adropin acts in brain to inhibit water drinking: potential interaction with the orphan G protein-coupled receptor, GPR19. American Journal of Physiology Regulatory, Integrative and Comparative Physiology 310(6):R476—R480.

[53] Thapa, D., Stoner, M.W., Zhang, M., Xie, B., Manning, J.R., Guimaraes, D., et al., 2018 Sep. Adropin regulates pyruvate dehydrogenase in cardiac cells via a novel GPCR-MAPK-PDK4 signaling pathway. Redox Biology 18:25—32.

[54] Ganesh Kumar, K., Zhang, J., Gao, S., Rossi, J., McGuinness, O.P., Halem, H.H., et al., 2012 Jul. Adropin deficiency is associated with increased adiposity and insulin resistance. Obesity 20(7):1394—1402.

[55] Chen, X., Chen, S., Shen, T., Yang, W., Chen, Q., Zhang, P., et al., 2020 Jun 24. Adropin regulates hepatic glucose production via PP2A/AMPK pathway in insulin-resistant hepatocytes. The FASEB Journal.

[56] Gao, S., McMillan, R.P., Zhu, Q., Lopaschuk, G.D., Hulver, M.W., Butler, A.A., 2015 Apr. Therapeutic effects of adropin on glucose tolerance and substrate utilization in diet-induced obese mice with insulin resistance. Molecular Metabolism 4(4):310—324.

[57] Chen, X., Xue, H., Fang, W., Chen, K., Chen, S., Yang, W., et al., 2019 Feb. Adropin protects against liver injury in nonalcoholic steatohepatitis via the Nrf2 mediated antioxidant capacity. Redox Biology 21:101068.

[58] Gao, S., McMillan, R.P., Jacas, J., Zhu, Q., Li, X., Kumar, G.K., et al., 2014 Oct. Regulation of substrate oxidation preferences in muscle by the peptide hormone adropin. Diabetes 63(10):3242—3252.

[59] Altamimi, T.R., Gao, S., Karwi, Q.G., Fukushima, A., Rawat, S., Wagg, C.S., et al., 2019 Sep. Adropin regulates cardiac energy metabolism and improves cardiac function and efficiency. Metabolism 98:37—48.

[60] Banerjee, S., Ghoshal, S., Stevens, J.R., McCommis, K.S., Gao, S., Castro-Sepulveda, M., et al., 2020 Oct 2. Hepatocyte expression of the micropeptide adropin regulates the liver fasting response and is enhanced by caloric restriction. Journal of Biological Chemistry 295(40):13753—13768.

[61] Kolben, Y., Weksler-Zangen, S., Ilan, Y., 2021. Adropin as a potential mediator of the metabolic system-autonomic nervous system-chronobiology axis: implementing a personalized signature-based platform for chronotherapy. Obesity Reviews 22(2):e13108.

[62] Chen, S., Zeng, K., Liu, Q.-C., Guo, Z., Zhang, S., Chen, X.-R., et al., 2017. Adropin deficiency worsens HFD-induced metabolic defects. Cell Death & Disease 8(8) e3008-e.

[63] Varikasuvu, S.R., Reddy, E.P., Thangappazham, B., Varshney, S., Das, V.L., Munikumar, M., 2021 Jul. Adropin levels and its associations as a fat-burning hormone in patients with polycystic ovary syndrome: a correlational meta-analysis. Gynecological Endocrinology 9:1—6.

[64] Beigi, A., Shirzad, N., Nikpour, F., Nasli Esfahani, E., Emamgholipour, S., Bandarian, F., 2015. Association between serum adropin levels and gestational diabetes mellitus; a case—control study. Gynecological Endocrinology 31(12):939—941, 2015/12/02.

[65] Nergiz, S., Altinkaya, S.O., Kurt Ömürlü, İ., Yuksel, H., Küçük, M., Demircan Sezer, S., 2015. Circulating adropin levels in patients with endometrium cancer. Gynecological Endocrinology 31(9):730—735, 2015/09/02.

[66] Ghoshal, S., Stevens, J.R., Billon, C., Girardet, C., Sitaula, S., Leon, A.S., et al., 2018. Adropin: an endocrine link between the biological clock and cholesterol homeostasis. Molecular Metabolism 8:51—64, 2018/02/01/.

[67] St-Onge, M.-P., Shechter, A., Shlisky, J., Tam, C.S., Gao, S., Ravussin, E., et al., 2014. Fasting plasma adropin concentrations correlate with fat consumption in human females. Obesity 22(4):1056—1063.

[68] Sayegh, M., Farquharson, A., Horgan, G., Ranawana, V., Drew, J.E., 2020. Postprandial adropin responses in women co-ingesting green leafy vegetables with a carbohydrate meal: interactions with the sirtuin system. Proceedings of the Nutrition Society 79(OCE3):E744.

[69] Han, S.I., Komatsu, Y., Murayama, A., Steffensen, K.R., Nakagawa, Y., Nakajima, Y., et al., 2014 May. Estrogen receptor ligands ameliorate fatty liver through a nonclassical estrogen receptor/Liver X receptor pathway in mice. Hepatology 59(5):1791—1802.

[70] Della Torre, S., Benedusi, V., Pepe, G., Meda, C., Rizzi, N., Uhlenhaut, N.H., et al., 2021. Dietary essential amino acids restore liver metabolism in ovariectomized mice via hepatic estrogen receptor α. Nature Communications 12(1):6883, 2021/11/25.

[71] Guillaume, M., Riant, E., Fabre, A., Raymond-Letron, I., Buscato, M., Davezac, M., et al., 2019 Jul. Selective liver estrogen receptor α modulation prevents steatosis, diabetes, and obesity through the anorectic growth differentiation factor 15 hepatokine in mice. Hepatology communications 3(7): 908—924.

[72] Chusyd, D.E., Wang, D., Huffman, D.M., Nagy, T.R., 2016. Relationships between rodent white adipose fat pads and human white adipose fat depots. Front Nutrition 3:10.

[73] Martin, M., 2011. Cutadapt removes adapter sequences from high-throughput sequencing reads. EMBnet. Journal 17(1):3 [next generation sequencing; small RNA; microRNA; adapter removal]. 2011 2011-05-02.

[74] Dobin, A., Davis, C.A., Schlesinger, F., Drenkow, J., Zaleski, C., Jha, S., et al., 2013 Jan 1. STAR: ultrafast universal RNA-seq aligner. Bioinformatics 29(1): 15—21.

[75] Anders, S., Pyl, P.T., Huber, W., 2015 Jan 15. HTSeq—a Python framework to work with high-throughput sequencing data. Bioinformatics 31(2):166—169.

[76] Love, M.I., Huber, W., Anders, S., 2014. Moderated estimation of fold change and dispersion for RNA-seq data with DESeq2. Genome Biology 15(12):550.

[77] Subramanian, A., Tamayo, P., Mootha, V.K., Mukherjee, S., Ebert, B.L., Gillette, M.A., et al., 2005 Oct 25. Gene set enrichment analysis: a knowledge-based approach for interpreting genome-wide expression profiles. Proceedings of the National Academy of Sciences of the United States of America 102(43):15545—15550.

[78] Li, H., Durbin, R., 2009 Jul 15. Fast and accurate short read alignment with Burrows-Wheeler transform. Bioinformatics 25(14):1754—1760.

[79] Langmead, B., Trapnell, C., Pop, M., Salzberg, S.L., 2009. Ultrafast and memory-efficient alignment of short DNA sequences to the human genome. Genome Biology 10(3):R25, 2009/03/04.

[80] Vlachos, I.S., Zagganas, K., Paraskevopoulou, M.D., Georgakilas, G., Karagkouni, D., Vergoulis, T., et al., 2015 Jul 1. DIANA-miRPath v3.0: deciphering microRNA function with experimental support. Nucleic Acids Research 43(W1):W460—W466.

[81] Karagkouni, D., Paraskevopoulou, M.D., Chatzopoulos, S., Vlachos, I.S., Tastsoglou, S., Kanellos, I., et al., 2018 Jan 4. DIANA-TarBase v8: a decade-long collection of experimentally supported miRNA-gene interactions. Nucleic Acids Research 46(D1):D239—D245.

[82] Shannon, P., Markiel, A., Ozier, O., Baliga, N.S., Wang, J.T., Ramage, D., et al., 2003 Nov. Cytoscape: a software environment for integrated models of biomolecular interaction networks. Genome Research 13(11):2498—2504.

[83] Patek, P.Q., Collins, J.L., Cohn, M., 1978 Nov 30. Transformed cell lines susceptible or resistant to in vivo surveillance against tumorigenesis. Nature 276(5687):510—511.

[84] Mehlem, A., Hagberg, C.E., Muhl, L., Eriksson, U., Falkevall, A., 2013. Imaging of neutral lipids by oil red O for analyzing the metabolic status in health and disease. Nature Protocols 8(6):1149—1154, 2013/06/01.

[85] Kurt, Z., Barrere-Cain, R., LaGuardia, J., Mehrabian, M., Pan, C., Hui, S.T., et al., 2018 Oct 22. Tissue-specific pathways and networks underlying sexual dimorphism in non-alcoholic fatty liver disease. Biology of Sex Differences 9(1):46.

[86] Chen, K.L.A., Zhao, Y.C., Hieronymi, K., Smith, B.P., Madak-Erdogan, Z., 2017. Bazedoxifene and conjugated estrogen combination maintains metabolic homeostasis and benefits liver health. PLoS One 12(12):e0189911.

[87] Hart-Unger, S., Arao, Y., Hamilton, K.J., Lierz, S.L., Malarkey, D.E., Hewitt, S.C., et al., 2017 Jun. Hormone signaling and fatty liver in females: analysis of estrogen receptor α mutant mice. International Journal of Obesity 41(6):945—954.

[88] Kittler, R., Zhou, J., Hua, S., Ma, L., Liu, Y., Pendleton, E., et al., 2013 Feb 21. A comprehensive nuclear receptor network for breast cancer cells. Cell Reports 3(2):538—551.

[89] Rakhshandehroo, M., Hooiveld, G., Muller, M., Kersten, S., 2009 Aug 27. Comparative analysis of gene regulation by the transcription factor PPARalpha between mouse and human. PLoS One 4(8):e6796.

[90] Gordon, F.K., Vallaster, C.S., Westerling, T., Iyer, L.K., Brown, M., Schnitzler, G.R., 2014 Aug. Research resource: aorta- and liver-specific ERalpha-binding patterns and gene regulation by estrogen. Molecular Endocrinology 28(8):1337—1351.

[91] Zhang, Y., Liu, T., Meyer, C.A., Eeckhoute, J., Johnson, D.S., Bernstein, B.E., et al., 2008. Model-based analysis of ChIP-seq (MACS). Genome Biology 9(9): R137.

[92] Collins, J.M., Huo, Z., Wang, D., 2021 Feb 2. ESR1 ChIP-seq identifies distinct ligand-free ESR1 genomic binding sites in human hepatocytes and liver tissue. International Journal of Molecular Sciences 22(3).

[93] Heinz, S., Benner, C., Spann, N., Bertolino, E., Lin, Y.C., Laslo, P., et al., 2010 May 28. Simple combinations of lineage-determining transcription factors prime cis-regulatory elements required for macrophage and B cell identities. Molecular Cell 38(4):576—589.